α-Al_2O_3 to γ-Al_2O_3 transition could occur would then be the melting point, so the change in Gibbs free energy ΔG of the α-Al_2O_3 to γ-Al_2O_3 transition would be zero at 2327 K. Taking the enthalpy of the α-Al_2O_3 to γ-Al_2O_3 transition as 13.4 kJ mol^{-1} (*11*), $\Delta S_{\alpha \to \gamma}$ is 5.7 J K^{-1} mol^{-1}.

11. J. M. McHale, A. Navrotsky, A. J. Perrotta, *J. Phys. Chem. B* **101**, 603 (1997).
12. G. F. Cerofolini, *Surf. Sci.* **51**, 333 (1975).
13. A. J. Perrotta *et al.*, unpublished material.
14. R.-S. Zhou and R. L. Snyder, *Acta Crystallogr. B* **47**, 617 (1991).
15. D. J. Coster, J. J. Fripiat, M. Muscas, A. Auroux, *Langmuir* **11**, 2615 (1995).
16. A. Gervasini and A. Auroux, *J. Phys. Chem.* **97**, 2628 (1993).
17. Hysteresis in adsorption isotherms, which implies a difference between the heats of adsorption and desorption, has been observed [see, for example, A. Bailey *et al.*, *Trans. Faraday Soc.* **67**, 231 (1971)]. However, these phenomena are usually associated with porous adsorbates, where irreversible changes in the pore structure occur upon adsorption. For the relatively nonporous aluminas considered here, the assumption that the heat of adsorption is the negative of the heat of desorption should be valid.
18. A. Navrotsky, *Phys. Chem. Miner.* **2**, 89 (1977).
19. This value was also proved to be accurate for the physisorbed H_2O in our previous study (*11*).
20. B. D. Begg, E. R. Vance, J. Nowotny, *J. Am. Ceram. Soc.* **77**, 3186 (1994).
21. H. F. Holmes, E. L. Fuller Jr., R. B. Gammage, *J. Phys. Chem.* **76**, 1497 (1972).
22. This work was supported by the Aluminum Company of America and NSF grants DMR 95-00812 and DMR 92-15802. We thank I. Aksay for the use of his BET surface-area–measuring equipment.

2 May 1997; accepted 17 June 1997

The Effect of Pressure on Deuterium-Hydrogen Fractionation in High-Temperature Water

T. Driesner*

The pressure dependence of deuterium-hydrogen (D-H) fractionation in water to 500°C and 200 megapascals has been calculated from high-temperature, high-pressure spectroscopic data. Pressure effects have a maximum at the critical temperature of water (20 per mil between 22 and 200 megapascals). Even larger effects are predicted for vaporlike densities from molecular dynamics simulations and molecular orbital calculations. Pressure effects explain many of the large discrepancies in published mineral-water D-H fractionation curves. Possible applications to natural examples include mineral-water isotope geobarometry.

The stable isotopes of oxygen and hydrogen have been the most commonly used geochemical tracers in the study of both fossil and modern fluid-rock interaction processes for more than 30 years (*1*). The most fundamental prerequisite for a successful application of D/H and $^{18}O/^{16}O$ ratios to the reconstruction of fluid sources, fluid quantities, flow directions, or stable-isotope geothermometry is the experimental or theoretical determination of accurate mineral-fluid isotope fractionation factors (*2*).

From statistical mechanical expressions that were derived in the 1940s to calculate equilibrium constants for isotope-exchange reactions between molecular species (*3*), it appeared that the equilibrium constants (and hence, fractionation factors) are a function of temperature only, because for free molecules and solid phases (that is, the favorite objects of theoretical studies and isotope geothermometry, respectively), the vibrational frequencies do not change significantly with pressure. Only for large pressure differences of several gigapascals, shifts of the vibrational frequencies of solids may lead to measurable effects on isotope fractionation (*4*).

However, unlike the case of solids, the vibrational frequencies of water undergo significant changes even at low to moderate pressures at temperatures of interest to many fields of stable-isotope geochemistry (*5–9*). Hence, at any given temperature, the fractionation of hydrogen (and oxygen) stable isotopes in systems involving water must be pressure dependent. Here, I quantify the pressure dependence and demonstrate its geochemical importance.

Inspection of the characteristics of the water spectra reveals that the effect of pressure on the D-H isotope fractionation in water may be quantified in a good approximation, even though only parts of the spectrum have been studied at elevated temperatures and pressures. This is possible because only the changes in the reduced partition function ratio of water with increasing pressure at a given temperature need to be calculated, rather than the complete reduced partition function.

The reduced partition function ratio of water can be split into the various contributions by

$$(Q_D/Q_H)_{total} = (Q_D/Q_H)_{stretch}(Q_D/Q_H)_{bend}(Q_D/Q_H)_{lib} \quad (1)$$

with subscripts denoting stretching, bending, and librational modes. Each of the terms is in turn a product of the reduced partition function ratios of several individual bands, for example, for *n* O-H stretching modes ν:

$$(Q_D/Q_H)_{stretch} = \prod_{\nu=1}^{n} (Q_D/Q_H)_\nu \quad (2)$$

A convenient definition of the pressure effect Γ_p is (*10*)

$$\Gamma_P = (Q_D/Q_H)_{total,P(ref)}/(Q_D/Q_H)_{total,P} \quad (3)$$

with subscript *P*(ref) denoting a reference pressure and *P* the pressure of interest. Then, substitution of Eqs. 1 and 2 into Eq. 3 shows that the contributions of all frequency bands that do not shift with pressure will cancel out in the calculation of Γ_p. Hence, only a simple spectral model rather than a full model of the vibrational density of states is required to calculate the pressure effect (*11*).

Using Eq. 3, I calculated the pressure effect to 500°C and 200 MPa. The results indicate a significant pressure effect at all temperatures. The curves in Fig. 1A are smoothed to remove undulations on the order of 1 unit in 1000 ln Γ_p (that is, 1 per mil in δD) resulting from the limited precision of the spectroscopic data. The strongest effects are observed at near-critical temperatures and pressures below about 100 MPa (*12*). This becomes more obvious when the results are plotted as contour lines of equal pressure effect in a *P-T* diagram (Fig. 1B). Whereas the variations are rather small below 350°C, steep gradients can be seen between 350° and 450°C. This result is not surprising, because most physical properties of water show small gradients in the low-temperature region and steep gradients near the critical point that are reduced at higher temperatures (*13*).

The practical usage of Fig. 1B is that to determine the effect of pressure on a mineral-water equilibrium fractionation factor at a given temperature, the difference between the contour lines at any two pressures has to be added to the fractionation factor when going up in pressure, or subtracted when going down.

To estimate the effect of pressure on the fractionation of the other important pair of stable isotopes in fluid-rock interaction studies ($^{18}O/^{16}O$), I carried out similar calculations using the data of Frantz *et al.* (*5*), and assuming that the O-H stretching fre-

---

Institut für Mineralogie und Petrographie, Eidgenössische Technische Hochschule–Zentrum, CH-8092 Zürich, Switzerland.

*Present address: Department of Chemical Engineering, The University of Tennessee, 419 Dougherty Building, Knoxville, TN 37996-2200, USA.

quencies shifted by a factor of 0.996 on substitution of ^{18}O for ^{16}O. The maximum effects are on the order of 0.4 per mil, and the contour lines closely follow the topology obtained for D-H fractionation. These low values explain why the only experimental study about pressure effects on ^{18}O-^{16}O fractionation did not find any measurable effects: Clayton *et al.* (*14*) carried out their studies at 500°C above 0.1 GPa where pressure effects can be expected to be small (less than about 0.2 per mil over the range of pressures of their study). In general, the pressure effect on ^{18}O-^{16}O fractionation in pure water is small and will hardly be detectable in natural samples.

I reviewed the available experimental mineral-water D-H fractionation curves to find experimental evidence for pressure effects, to check the accuracy of the present results, and to possibly resolve the huge discrepancies between the individual calibrations, as well as to understand the unusual shape of many of the calibration curves. Evidence for pressure effects of the same magnitude as calculated was found for most experimentally studied mineral-water fractionations. The epidote-water calibrations will be discussed as an example. Two data sets are available: Graham *et al.* (*15*) did their experiments at 200 MPa and 150° to 400°C, and at 400 MPa and 250 to 650°C, by direct epidote-water exchange. Vennemann and O'Neil (*16*) used an indirect determination by H_2-epidote equilibration at 0.3 to 2 bars.

The two calibrations differ from about 15 per mil at 200°C to almost 70 per mil at 400°C. Vennemann and O'Neil (*16*) combined their low-pressure epidote-H_2 fractionation factors with low-pressure experimental (*17*) or theoretical H_2-H_2O fractionation factors (*18*), respectively. They assumed that this gives an epidote–water vapor fractionation that can be combined with experimental water liquid-vapor fractionation factors (*19*) to calculate the epidote-liquid water fractionation. However, there are two steps missing in this approach to compare their results with Graham *et al.* (*15*). First, the theoretical H_2-H_2O fractionation of Richet *et al.* (*18*) that they used applies to an ideal water vapor consisting of water monomers only. The real water vapor at the liquid-vapor curve above about 200°C, however, is quite dense and consists of water clusters (dimer, trimer, . . .) (*20*) that fractionate D-H differently. This is equivalent to a density (and hence pressure) effect on isotope fractionation in the vapor phase. Because no experimental data are available, molecular dynamics simulations were used to determine the abundance of clusters in the vapor phase, and ab initio methods were used to calculate the vibra-

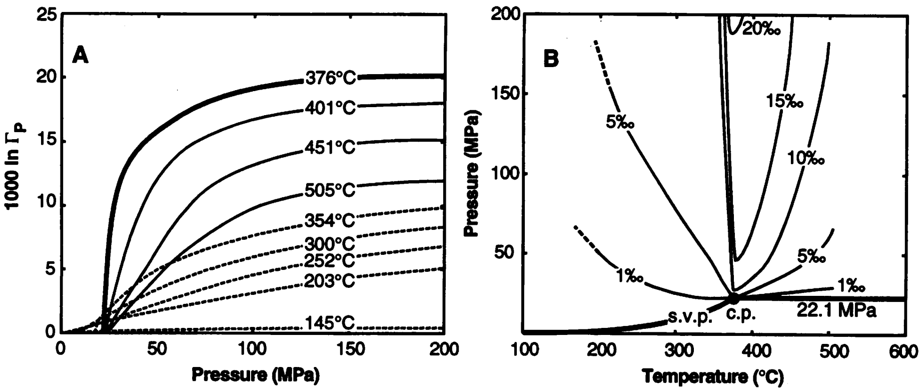

Fig. 1. Pressure effect on D-H fractionation in high-temperature water. (**A**) Pressure effect as defined in Eq. 3 for various temperatures [calculated from Raman data of Frantz *et al.* (*5*) and Kohl (*6*)]. (**B**) Contour lines of the pressure effect in a *P-T* diagram. Values are relative to saturated vapor pressure (s.v.p) below the critical point (c.p.) and relative to the critical pressure (22.1 MPa) above.

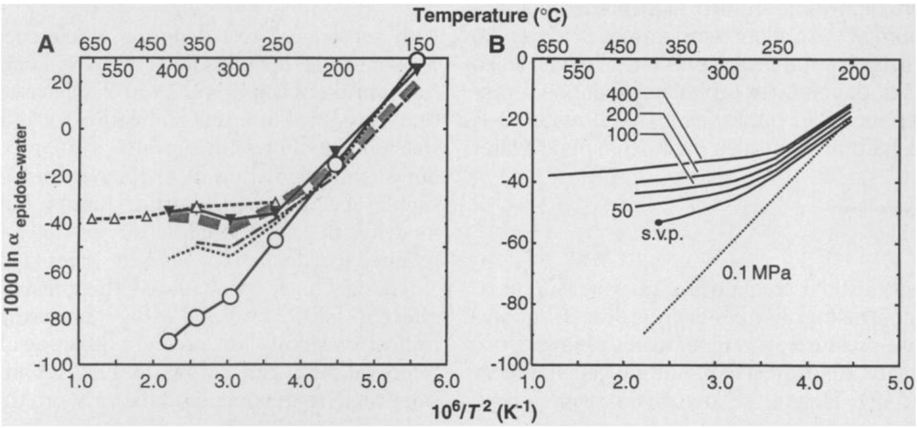

Fig. 2. Epidote-water D-H fractionation. (**A**) Comparison between Vennemann and O'Neil (V and O) data (*16*) and Graham *et al.* (*15*). Solid line with open circles: V and O epidote-vapor; data "points" at 200° and 350°C are interpolations. Dotted, dash-dotted line, and thick gray dashed line show stepwise correction procedure to V and O epidote-vapor curve. Dotted line: V and O + ideal-real vapor correction; dash-dotted line: V and O + ideal-real vapor + liquid-vapor corrections; thick gray dashed line: V and O after complete correction (ideal-real + liquid-vapor + pressure effect from Fig. 1). Agreement with the 200 MPa curve of Graham *et al.* (solid line, black triangles) is excellent. The 400 MPa curve of Graham *et al.* (dashed line, open triangles) is shown for comparison. Symbol size and thickness of gray dashed line refer to uncertainties in 1000 ln $\alpha_{epidote\text{-}water}$. (**B**) Epidote-water D-H fractionation as a function of pressure and temperature with the experimental results of Graham *et al.* (*15*), Vennemann and O'Neil (*16*), and the results of the present study. Minor uncertainties have been smoothed. Curve labels denote pressure in MPa (s.v.p., saturated vapor pressure).

Table 1. Theoretical D-H fractionation in high-temperature water vapor. Values are the fraction (in percent) of the denoted species in the vapor phase as derived from molecular dynamics simulations (*21*). Numbers in parentheses are D-H fractionations 1000 ln $\alpha_{cluster\text{-}monomer}$ as obtained from density functional calculations of the vibrational spectra of the clusters (*21*). The factor 1000 ln $\alpha_{vapor\text{-}monomer}$ is directly calculated from these data (assuming that the D-H fractionation of higher clusters can be taken as similar to that of the hexamer). Uncertainties in 1000 ln $\alpha_{vapor\text{-}monomer}$ result mainly from uncertainties in the fractions of the clusters (*21*).

Temperature (°C) Density (g cm^{-3})	200 0.005	250 0.02	300 0.06	350 0.11	400 0.13
Monomer	86 (0)	66 (0)	40 (0)	27 (0)	22 (0)
Dimer	9 (+16)	16 (+11)	18 (+8)	18 (+6)	15 (+2)
Trimer	2 (+19)	6 (+10)	9 (+3)	12 (−2)	10 (−4)
Tetramer	0.7 (0)	3 (−9)	5 (−15)	9 (−18)	8 (−20)
Pentamer	0.3 (−11)	2 (−18)	3 (−23)	7 (−26)	7 (−29)
Hexamer and higher	1.5 (−115)	7 (−111)	15 (−106)	27 (−101)	38 (−94)
1000 lnα (vapor-monomer)	+2 ± 1	−6 ± 1	−17 ± 2	−30 ± 3	−39 ± 5

tional frequencies and hence the isotope fractionation of the various clusters (*21*). The results are summarized in Table 1. Second, pressure effects in the liquid as derived above have to be taken into account. As shown in Fig. 2A, the agreement of the two data sets after the correction steps is excellent (*22*). Figure 2B shows the position of the fractionation curve for various pressures. The subhorizontal section above about 300°C points to a possible geobarometer.

The calculated pressure effects have also been applied to other published mineral-water fractionations and appear to quantitatively explain the apparent discrepancies in the fractionation curves for muscovite (*16*, *23*), hornblende (*16*, *23*, *24*), boehmite (*15*, *23*), kaolinite above 200°C (*16*, *25*), and possibly also biotite (*16*, *23*). Furthermore, they also explain why most experimental D-H fractionation curves do not follow the simple $1/T^2$ temperature dependence. This dependence was predicted for phases and species with a fixed set of frequencies (*3*), which is not true for most of the experiments because the water frequencies change with temperature and pressure. Most "unusual" mineral-water fractionation curves (*15*, *16*, *23*–*26*) show a normal behavior when they are corrected to a pressure of 1 bar with the present results.

The impact of these results pertains to many applications of stable-isotope geochemistry. Until now, the choice of an appropriate fractionation curve was subject to the researcher's preferences, and hence the interpretation of field data was unavoidably biased (if a choice between different curves had to be done) or quantitatively in error (depending on the pressure difference between the actual field example and the laboratory calibration). This is of particular importance for the application to the reconstruction of fluid sources. The pressure effects (up to 20 per mil) and the effects of dissolved salts on hydrogen stable-isotope fractionation in aqueous solutions [up to 30 per mil at salt saturation (*10*, *27*)] are additive. Thus, the present models derived for the origin of highly saline fluids at low to moderate pressures should be reconsidered. The effects could be particularly important in interpreting the early stages of development of porphyry copper deposits, which have highly saline fluids in the temperature range between 350° and 450°C and possible large pressure fluctuations, for example, during boiling.

The definitions of magmatic water types and genetic interpretations may also be affected, because some of these are based on application of mineral-water fractionation factors. Pressure effects may become significant during the release of fluids in subduction zones and the subsequent formation of arc magmas. Also, many geothermal systems are operating at temperature-pressure conditions where the largest pressure effects are to be expected. Particularly large errors when applying high-pressure mineral-water calibrations are to be expected in vapor-dominated (or even undersaturated) zones where strong variations in δD at near constant $\delta^{18}O$ may occur.

The results also imply that the isotope fractionation curves (commonly taken as "pressure independent") have the potential to be a sensitive geobarometer in the low- to medium-pressure region above about 300°C. However, difficulties with natural samples (for example, retrograde exchange, inhomogeneities, and knowledge of the fluid's isotopic composition) may exclude this from becoming a routine tool. If pressure effects in the liquid and vapor phases are carefully calibrated by conventional hydrothermal techniques for one mineral (for example, epidote), the resulting data can be used directly in combination with the innovative H_2 equilibration technique of Vennemann and O'Neil (*16*) to derive the complete pressure-temperature systematics of D-H fractionation of other minerals.

Hence, we may be optimistic that the whole of mineral-water isotope fractionation systematics can successfully be studied experimentally within a relatively short time in the near future. Although the discovery of large pressure effects complicates the interpretation of hydrogen isotope data, it also shows that stable-isotope signals in natural rock and mineral samples carry even more information than previously thought.

REFERENCES AND NOTES

1. H. Craig, in *Nuclear Geology of Geothermal Areas* (Consiglio Nazionale delle Ricerche, Pisa, Italy, 1963), p. 17. For reviews of the application of stable isotopes to the study of fluid-rock interaction, see *Rev. Mineral.* **16**, 165 (1986).
2. The fractionation factor describes the distribution of isotopes between two phases or species and is defined as $\alpha_{A\text{-}B} = R_A/R_B$, where *R* denotes the concentration ratio of the heavy and light isotope (for example, D/H or $^{18}O/^{16}O$) in the phase or species A or B. Values of the fractionation factor are given in the 1000 ln α notation. The typically required accuracy is 1 to 2 per mil for D-H and 0.1 to 0.2 per mil for $^{18}O\text{-}^{16}O$ fractionation factors.
3. H. C. Urey, *J. Chem. Soc. (London)*, 562 (1947); J. Bigeleisen and M. G. Mayer, *J. Chem. Phys.* (1947). The most commonly applied expression uses the reduced partition function ratio for the isotopically substituted molecule:

$$Q_h/Q_l = (\sigma_l/\sigma_h)(m_h/m_l)^{3/2} \prod_{i=1}^{3N-6} (U_{hi}/U_{li}) \\ (e^{-U_{hi}/2}/e^{-U_{li}/2})(1 - e^{-U_{li}}/1 - e^{-U_{hi}}) \qquad (4)$$

where *Q* is the reduced partition function (subscript h for the heavy, l for the light isotope), σ denotes the symmetry number, *m* is the atomic mass of the isotope of interest, and *U* is an abbreviation for $h\nu/kT$ (*h*: Planck's constant; ν: vibrational frequency; *k*: Boltzmann's constant; *T*: temperature in Kelvin). The first two terms are the translational and rotational contributions to the reduced partition function ratio, which for the purpose of the present study can be taken as classical, hence not contributing to isotopic fractionation. The other terms are the vibrational contributions treated in the harmonic approximation. Thus, in a very good approximation, there are only two variables that determine the magnitude of isotope fractionation, that is, temperature and the vibrational frequencies. From the reduced partition functions of any two phases or species A and B, the equilibrium constant for the isotope exchange between these can be calculated as $K_{A\text{-}B} = (Q_h/Q_l)_A\ (Q_h/Q_l)_B$. In most cases, $K_{A\text{-}B}$ is numerical identical to $\alpha_{A\text{-}B}$. If not, a simple practical way to calculate $\alpha_{A\text{-}B}$ is to leave out the symmetry number terms. For a detailed discussion, see V. I. Ferronsky and V. A. Polyakov, *Environmental Isotopes in the Hydrosphere* (Wiley, Chicester, UK, 1982), pp. 14–43.
4. V. B. Polyakov and N. N. Kharlashina, *Geochim. Cosmochim. Acta* **58**, 4739 (1994).
5. J. D. Frantz, J. Dubessy, B. Mysen, *Chem. Geol.* **106**, 9 (1993).
6. W. Kohl, thesis, Univ. of Karlsruhe, Germany (1989).
7. H. A. Lindner, thesis, Univ. of Karlsruhe, Germany (1970).
8. C. I. Ratcliffe, D. E. Irish, *J. Phys. Chem.* **86**, 4897 (1982).
9. D. L. Farber, Q. Williams, E. Knittle, *Eos Trans. Am. Geophys. Union* **71**, 1600 (1990).
10. For consistency with the conventions used in recent work on the changes in the isotope activity ratios in water on the addition of salts [J. Horita, D. R. Cole, D. J. Wesolowski, *Geochim. Cosmochim. Acta* **59**, 1139 (1995)], the pressure effect was given the sign Γ_p and the ratio was set up in the order as given in Eq. 3.
11. The spectral models were composed on the assumption that pressure-dependent modes occur in the stretching, bending, and librational regions. Saturated vapor pressure was chosen as the reference pressure below the critical temperature and critical pressure (22.1 MPa) above. Detailed information is available for the stretching region. According to Frantz *et al.* (*5*), the O-H stretching region can be split into six bands, D_1 to D_6. Only the D_3 and D_4 bands show significant temperature and pressure dependences and have to be incorporated into the model. A $\nu_{O\text{-}D}/\nu_{O\text{-}H}$ ratio of 0.745 was assumed on the basis of the data of Frantz *et al.* (*5*) and Kohl (*6*). For the bending region, spectroscopic data (*6*, *8*, *9*) and molecular dynamics simulations [A. Kalinichev and K. Heinzinger, *Geochim. Cosmochim. Acta* **59**, 641 (1995)] indicate large blueshifts with pressure. With the use of these data, it was assumed that at 200 MPa and above, the bending frequency is close to that in liquid water at ambient conditions (1645 cm^{-1}) and does not decrease below the gas phase value (1595 cm^{-1}) in the low-pressure region. One H-O-H mode with a $\nu_{H\text{-}O\text{-}D}/\nu_{H\text{-}O\text{-}H}$ of 0.846 was used. Blueshifts in the librational modes with increasing pressure are expected in the high-temperature region due to the effect of density changes on the intermolecular forces. This view is supported by the temperature dependence of the librational modes as observed in molecular dynamics simulations along the liquid-vapor curve [J. Marti *et al.*, *J. Chem. Phys.* **105**, 639 (1996)]. A large blueshift of 20 cm^{-1} per 0.1 g cm^{-1} density increase was assigned to a single mode with a position at 600 cm^{-1} at 200 MPa. The bending and librational blueshifts used possibly overemphasize the contributions of these modes. Anharmonicity effects were not taken into account but—if important—are likely to reduce the contribution of the librational modes. In addition to the simple model of two stretching, one bending, and one librational mode, several other models with additional bands in all three regions were tested but gave very similar results. The qualitative picture shown in Fig. 1 is independent of the spectral model. Reducing the contributions from the bending and librational modes results in larger pressure effects at high temperature. Figure 1 is thus regarded as a conservative estimate of the magnitude of the pressure effects above the reference pressure.
12. This indicates that the effects should be understood in terms of density rather than pressure, because the

strongest pressure dependence parallels the strongest density changes (and hence the strongest changes in molecular interactions). Because fluid pressure rather than density is the commonly used variable in geochemistry, the relation to pressure has been kept throughout the present communication.

13. L. Haar, J. S. Gallagher, G. S. Kell, *NBS/NRC Steam Tables* (1983).
14. R. N. Clayton *et al.*, *Geochim. Cosmochim. Acta* **39**, 1197 (1975).
15. C. M. Graham, S. M. F. Sheppard, T. H. Heaton, *ibid.* **44**, 353 (1980).
16. T. W. Vennemann and J. R. O'Neil, *ibid.* **60**, 2437 (1996).
17. H. E. Suess, *Z. Naturforsch.* **4a**, 328 (1949); E. Cerrai *et al.*, *Chem. Eng. Prog. Symp. Ser.* **50**, 271 (1958).
18. P. Richet, Y. Bottinga, M. Javoy, *Annu. Rev. Earth Planet. Sci.* **5**, 65 (1977).
19. J. Horita and D. J. Wesolowski, *Geochim. Cosmochim. Acta* **58**, 3425 (1994).
20. Evidence for such clusters comes from the low-pressure Raman spectra of Frantz *et al.* (*5*), as well as from molecular dynamics simulations [Y. Guissani and B. Guillot, *J. Chem. Phys.* **98**, 8221 (1993)].
21. The molecular dynamics simulations were carried out with the SPC/E water model that has been shown to accurately reproduce the liquid-vapor curve and the critical parameters as well as many other properties of real water [Y. Guissani and B. Guillot, *J. Chem. Phys.* **98**, 8221 (1993); J. Alejandre, D. J. Tildesley, G. A. Chapela, *ibid.* **102**, 4574 (1994)]. Simulations were done with 1000 SPC/E water molecules in a cubic box with periodic boundary conditions in the NVT ensemble. Densities were chosen according to the two studies mentioned above. Long-range forces were treated with Ewald summation. Systems were allowed to equilibrate for at least 25 ps, and simulation runs were at least 50 ps. When calculating the fractions of the various clusters from the positions of the molecules in the simulation box, geometrical criteria for the identification of the clusters were applied. It was assumed that a molecule belongs to a cluster when its oxygen is located within a distance smaller than the position of the first minimum of the oxgen-oxygen radial distribution function (typically 4.0 to 4.2 Å). The calculations of the vibrational spectra of the clusters were done with density functional methods as implemented in Gaussian94 (M. J. Frisch *et al.*, Gaussian94, Gaussian Inc., Pittsburgh, PA, 1995). The BLYP functional in combination with the 6-31G** basis set was used. This method yields precise frequencies that are numerically very close to the spectroscopic values [see, for example, A. P. Scott and L. Radom, *J. Phys. Chem.* **100**, 16502 (1996)]. For each cluster, after the geometry optimization, one calculation was carried out with ^{16}O and H only. Then, a series of calculations were carried out in each of which one of the various hydrogens was substituted by D. The fractionation relative to the monomer was calculated for all these various possibilities, and the arithmetic mean of the 1000 ln $\alpha_{\text{cluster-monomer}}$ was taken as the average cluster-monomer fractionation. Calculations at the MP2/6-31G** level gave essentially identical fractionation factors when the scaling factors given by Scott and Radom were used. The vapor-monomer fractionation is directly calculated from these results. Changing parameters like the geometric definition of clusters within reasonable limits indicate uncertainties in this approach of less than 5 per mil at 400°C and of about 1 per mil at 200°C.
22. Furthermore, pressure effects explain many details in the data set of Graham *et al.* (*15*) that otherwise are not understandable. At 250°C their 400-MPa fractionation curve lies ~4 to 5 per mil higher than the 200-MPa curve. A rough extrapolation of Fig. 1A to higher pressures predicts a similar, though slightly smaller, shift. At 350°C, the same equilibrium fractionation was measured for the two different pressures. Inspection of Fig. 1B reveals a straightforward explanation: At 200 MPa and 350°C, the contour lines of the pressure effect lie very close together, and a temperature variation of 5°C [the stated uncertainty of Graham *et al.* (*15*)] can cause a change in the fractionation by a few per mil.
23. T. Suzuoki and S. Epstein, *Geochim. Cosmochim. Acta* **40**, 1229 (1976). These authors did not give information about the pressure in their experiments, but in the light of the present results, their 400° and 450°C data are likely to have been generated at about 250 to 400 bars.
24. C. M. Graham, R. S. Harmon, S. M. F. Sheppard, *Am. Mineral.* **69**, 128 (1984).
25. H. A. Gilg and S. M. F. Sheppard, *Geochim. Cosmochim. Acta*, **60**, 3, 529 (1996).
26. R. E. Stoffregen, R. O. Rye, M. D. Wasserman, *ibid.* **58**, 903 (1994).
27. T. Driesner, thesis, Eidgenössische Technische Hochschule–Zürich (1996); K. Shmulovich *et al.*, *Terra Nova* **9**, 540 (1997).

10 April 1997; accepted 19 June 1997

Paleostress in Cratonic North America: Implications for Deformation of Continental Interiors

Ben A. van der Pluijm, John P. Craddock, Brita R. Graham, John H. Harris

Compressive paleostresses, as recorded by twinned calcite in carbonate rocks that cover cratonic northwestern North America, are perpendicular to the orogenic front of the Late Cretaceous to Early Cenozoic Sevier fold-thrust belt. Inferred differential stresses decrease from ~100 megapascals (MPa) at the orogenic front to ~20 MPa up to 2000 kilometers inland. New analyses near the Late Paleozoic Appalachian front refine earlier results from the eastern Midcontinent. The Appalachian and Sevier stress data in North America's continental interior are remarkably similar in spite of distinctly different tectonic properties. This suggests that continental interior stresses are largely insensitive to tectonic characteristics of compressive plate margins and that far-field stress transmission is filtered by deformation styles in mountain belts.

A basic tenet of plate tectonics is that deformation is concentrated at plate margins, whereas plate interiors are rigid and undeformable (*1*). This basic assumption is supported by many geologic observations, such as the location of major earthquake activity, certain types of volcanism, and present-day mountain-building processes. However, continental interiors are increasingly recognized as sensitive recorders of plate tectonic activity (*2*, *3*). For example, Late Paleozoic plate interactions at the Appalachian margin of North America produced fault reactivation, folds and detachments, and joint and cleavage fabrics in the eastern Midcontinent region of the United States (*4*, *5*). We present data from the western part of the continent, which is characterized by Mesozoic-Cenozoic convergence between the Farallon and North American plates that resulted in the formation of the Sevier fold-thrust belt (Sevier f., Fig. 1). In addition, we obtained results from a 300-km section in the eastern Midcontinent to better constrain the nature of paleostress decrease near orogenic fronts (Appalachian f., Fig. 1).

Our regional strain and paleostress history uses the twinning of calcite in limestone, cement, and veins of the Sevier fold-thrust belt and its foreland, younger basement-cored (Laramide) structures and old adjacent tectonic provinces. Calcite grains can twin mechanically at low differential stress (<20 MPa) in a crystal-plastic process that is largely independent of temperature and normal stress magnitude at shallow crustal conditions. Twinning occurs along one of three glide planes, and calcite strain-hardens once twins have formed; further twinning is possible along either of the remaining two planes at higher stresses, provided that stress is oriented >45° from the initial stress orientation (*6*).

The orientation (*7*) and magnitude of paleostresses responsible for twinning can be calculated (*8*); magnitude errors are within 20%. Strain determinations using the Groshong method (*9*) are quite accurate for finite strains less than ~15%. This method also computes negative and positive expected values (NEVs and PEVs, respectively) for all the twinned grains in a sample. A NEV indicates that a grain was unfavorably oriented relative to the stress that caused most of the other grains in a sample to twin. High NEV percentages (>35%) may indicate that a second, noncoaxial strain event occurred, and these two events can be analyzed separately. We only used samples that are characterized by low

---

B. A. van der Pluijm, B. R. Graham, J. H. Harris, Department of Geological Sciences, University of Michigan, Ann Arbor, MI 48109, USA.

J. P. Craddock, Geology Department, Macalester College, St. Paul, MN 55105, USA.